Neuro-Oncology
23(12), 2028–2041, 2021 | doi:10.1093/neuonc/noab127 | Advance Access date 28 May 2021

Carbon ion radiotherapy eradicates medulloblastomas with chromothripsis in an orthotopic Li-Fraumeni patient-derived mouse model

Milena Simovic, Michiel Bolkestein, Mahmoud Moustafa, John K. L. Wong, Verena Körber, Sarah Benedetto, Umar Khalid, Hannah Sophia Schreiber, Manfred Jugold, Andrey Korshunov, Daniel Hübschmann, Norman Mack, Stephan Brons, Pei-Chi Wei, Michael O. Breckwoldt, Sabine Heiland, Martin Bendszus, Jürgen Debus, Thomas Höfer, Marc Zapatka, Marcel Kool, Stefan M. Pfister, Amir Abdollahi, and Aurélie Ernst

Group Genome Instability in Tumors, German Cancer Research Center, (DKFZ), Heidelberg, Germany (M.S., M.B., U.K., H.S.S., A.E.); Faculty of Biosciences, Heidelberg University, Heidelberg, Germany (M.S., U.K.); Division of Molecular & Translational Radiation Oncology, Heidelberg Ion-Beam Therapy Center (HIT), Heidelberg, Germany (M.M., A.A.); Heidelberg Institute for Radiation Oncology (HIRO), Heidelberg, Germany (M.M., J.D., A.A.); National Center for Radiation Oncology (NCRO), Heidelberg, Germany (M.M., A.A.); National Center for Tumor Diseases (NCT), Heidelberg, Germany (M.M., J.D., A.A.); Heidelberg University Hospital (UKHD) and DKFZ, Heidelberg, Germany (M.M., A.A.); German Cancer Consortium (DKTK), Partner Site Heidelberg, DKFZ, Heidelberg, Germany (M.M., J.K.L.W., A.K., D.H., N.M., J.D., M.Z., M.K., S.M.P., A.A.); Department of Clinical Pathology, Suez Canal University, Ismailia, Egypt (M.M.); Division of Molecular Genetics, DKFZ, Heidelberg, Germany (J.K.L.W., N.M., M.Z.); Division of Theoretical Systems Biology, DKFZ, Heidelberg, Germany (V.K., S.B., T.H.); Faculty of Medicine, Heidelberg University, Heidelberg, Germany (H.S.S.); Core Facility, Small Animal Imaging Center, DKFZ, Heidelberg, Germany (M.J.); Clinical Cooperation Unit Neuropathology, DKFZ, Department of Neuropathology, UKHD, Heidelberg, Germany (A.K.); Computational Oncology Group, Molecular Diagnostics Program at the NCT and DKFZ, Heidelberg, Germany (D.H.); Heidelberg Institute for Stem cell Technology and Experimental Medicine, Heidelberg, Germany (D.H.); Department of Pediatric Oncology, Hematology and Immunology, UKHD, Heidelberg, Germany (D.H., N.M., S.M.P.); Hopp Children's Cancer Center, NCT Heidelberg (KiTZ), Heidelberg, Germany (N.M., M.K., S.M.P.); Division of Pediatric Neurooncology, DKFZ, Heidelberg, Germany (N.M, M.K., S.M.P.); Heidelberg Ion-Beam Therapy Center (HIT), Heidelberg, Germany (S.B.); Brain Mosaicism and Tumorigenesis, DKFZ, Heidelberg, Germany (P.-C.W.); Department of Neuroradiology, UKHD, Heidelberg, Germany (M.O.B., S.H., M.Be.); Department of Radiation Oncology, UKHD, Heidelberg, Germany (J.D.); Department of Radiation Oncology, Eberhard-Karls-University Tuebingen, Tübingen, Germany (J.D.); Clinical Cooperation Unit Radiation Oncology, DKFZ, Heidelberg, Germany (J.D.); Princess Máxima Center for Pediatric Oncology, Utrecht, Netherlands (M.K.)

Corresponding Author: Aurélie Ernst, German Cancer Research Center, INF 580, Heidelberg, Germany (a.ernst@dkfz.de).

Abstract

Background. Medulloblastomas with chromothripsis developing in children with Li-Fraumeni Syndrome (germline *TP53* mutations) are highly aggressive brain tumors with dismal prognosis. Conventional photon radiotherapy and DNA-damaging chemotherapy are not successful for these patients and raise the risk of secondary malignancies. We hypothesized that the pronounced homologous recombination deficiency in these tumors might offer vulnerabilities that can be therapeutically utilized in combination with high linear energy transfer carbon ion radiotherapy.

Methods. We tested high-precision particle therapy with carbon ions and protons as well as topotecan with or without PARP inhibitor in orthotopic primary and matched relapsed patient-derived xenograft models. Tumor and normal tissue underwent longitudinal morphological MRI, cellular (markers of neurogenesis and DNA damage-repair), and molecular characterization (whole-genome sequencing).

Results. In the primary medulloblastoma model, carbon ions led to complete response in 79% of animals irrespective of PARP inhibitor within a follow-up period of 300 days postirradiation, as detected by MRI and histology. No

sign of neurologic symptoms, impairment of neurogenesis or in-field carcinogenesis was detected in repair-deficient host mice. PARP inhibitors further enhanced the effect of proton irradiation. In the postradiotherapy relapsed tumor model, median survival was significantly increased after carbon ions (96 days) versus control (43 days, $P < .0001$). No major change in the clonal composition was detected in the relapsed model. **Conclusion.** The high efficacy and favorable toxicity profile of carbon ions warrants further investigation in primary medulloblastomas with chromothripsis. Postradiotherapy relapsed medulloblastomas exhibit relative resistance compared to treatment-naïve tumors, calling for exploration of multimodal strategies.

Key Point

- Carbon ions eradicate chromothriptic medulloblastoma in a preclinical mouse model.

Importance of the Study

Children developing medulloblastomas with chromothripsis have a very poor prognosis. Tightly linked with pathogenic germline variants in *TP53*, these aggressive brain tumors are challenging to treat by conventional photon radiotherapy and chemotherapy due to the risk of secondary malignancies. Particle radiation has not been extensively tested in pediatric (neuro-) oncology and in the context of germline predisposition. We hypothesized that the high precision provided by particle therapy might be utilized to eliminate medulloblastoma cells, while minimizing the damage to the surrounding brain tissue. Furthermore, the marked homologous recombination repair deficiency detected in these tumors might offer vulnerabilities that can be targeted by synthetically lethal interactions. We showed that carbon ions eradicate primary medulloblastoma cells with chromothripsis in preclinical patient-derived xenografts.

Chromothripsis is a recently identified form of genome instability, by which a one-off catastrophic event gives rise to massive genomic rearrangements of one or a few chromosome(s).[1,2] Generally regarded as an early event in tumor development, chromothripsis is thought to play a causative role in tumor initiation.[3–5] This phenomenon is frequently observed in cancer, occurring in more than 20% of cases in numerous cancer types.[6–9] In specific tumor entities and molecular subgroups, the prevalence of chromothripsis reaches up to 100%, such as for instance in medulloblastomas developing in children with Li-Fraumeni Syndrome (LFS).[1,10] Like in other malignant brain tumors and in a number of additional tumor types, chromothripsis is linked with poor prognosis in these patients,[10] who have limited treatment options, stressing the urgent need for innovative treatment modalities.

Due to the germline *TP53* mutation, local therapy intensification in these patients is limited by the risk of development of secondary malignancies, which could occur in 30%–50% of LFS cases, often within the radiation field.[11,12] Likewise, genotoxic chemotherapy can contribute to the development of subsequent tumors in the context of p53 dysfunction.[13] Therefore, maximal normal tissue sparing is a prerequisite for therapy intensification in this cancer entity.

Recent developments in high-precision radiotherapy utilizing protons and carbon ions (CIRT) offer a steep dose gradient and sparing of surrounding normal tissue.[14–16] The benefits of particle therapy alone or in combination with other modalities were shown in a number of tumor types.[17,18] In pediatric patients, particle therapy with heavy ions has not been extensively studied, and has been limited to few tumor types, such as inoperable osteosarcoma, rhabdomyosarcoma, or chordoma.[19,20] Even though these technologies are extremely powerful, the novelty and the potential risks linked to side-effects have slowed down their applications in pediatric (neuro-) oncology, in particular for heavier ions like carbon.

Synthetic lethality and sensitization approaches may allow using lower doses of radiation, limiting side-effects.[21] In the context of medulloblastomas with chromothripsis and p53 dysfunction, utilizing synthetically lethal interactions would decrease the risk for secondary tumors. Chromothripsis is tightly linked with DNA repair defects, and in particular with Homologous Recombination (HR) repair deficiency or BRCAness.[22,23] Importantly, HR deficiency may offer vulnerabilities to target tumor cells, as it makes cells potentially sensitive to radiation[24] and to Poly (ADP-ribose) polymerase (PARP) inhibition.[25,26] Synthetic lethality between *BRCA*-mutant tumors and pharmacologic inhibition of PARP first led to clinical trials in breast and ovarian cancer.[27,28] This strategy was then successfully extended to a range of tumor types such as gastric cancer, pancreatic cancer, small cell lung cancer, Ewing's sarcoma, melanoma, and glioblastoma, not only in the context of *BRCA* mutations but for tumors presenting molecular signatures of BRCAness.[29] Remarkably, PARP inhibitors (PARPi) were also identified as potent radiosensitizers[30–32] and showed promising results in the clinic as single treatment or combined with radiation or chemotherapy.[33]

Even though chromothripsis plays a major role in tumor development, no specific therapy has been developed for patients with chromothriptic tumors. Therefore, we set off to test particle therapy in medulloblastomas with chromothripsis, alone and in combination with the novel PARPi BGB290.

Materials and Methods

Cell Culture

DAOY cells were cultivated in DMEM high glucose (Gibco, #41965) with 10% FCS and 1% L-glutamine. For spheroid cultures, tumors were isolated from the mouse brains, homogenized by pipetting in NeuroCult™ NS-A Proliferation Kit (STEMCELL Technologies, #05751) and filtered to obtain single cell suspensions. To cultivate spheroids, 0.25–0.5 million cells were plated per 25 cm^2 flask (Greiner, #690195) in 10 ml media (see Supplementary Table 1).

In vitro Radiation and Drug Response

DAOY cells were seeded in 96-well plates (Corning, #3596) at a density of 5000 cells per well and treated 24 h later. For treatment with radiation and topotecan, see Supplementary Methods. Metabolic activity was analyzed 72 h after treatment start with MTT assays (Sigma-Aldrich, #M5655). Spheroids from patient-derived xenograft models (PDX) were treated with 5 µM Topotecan alone or combined with BGB290 (IC20 or IC40). Metabolic activity was measured after 96 h with ATPlite Luminescence assays (Perkin Elmer, #6016943).

Clinical Samples

Clinical samples and data were collected, after receiving written informed consent in accordance with the Declaration of Helsinki and approval from the respective institutional review boards.

Animal Studies

Orthotopic PDX mouse models were established in 6–10-week-old female immunocompromised mice (NSG, NOD.*Cg-Prkdc*^{scid}*Il2rg*^{tm1Wjl}). For the pilot radiation study, patient-derived cells were injected in mice of NOD.*Cg-Prkdc*^{scid}*Il2rg*^{tm1Wjl} (NSG, DKFZ breeding), *NOD.Cg-Rag1*^{tm1Mom}*Il2rg*^{tm1Wjl} (NRGS, DKFZ breeding) and *BALB/cAnNRj-Foxn1*$^{nu/nu}$ (BALB/c, Janvier). For all other experiments with PDX models, 6–10-week-old female NRGS mice were used. Patient-derived tumor cells were injected into the cerebellum, as described previously.[34] Tumor growth was followed by MRI and animals were randomized into treatment groups based on tumor volume measurements. For radiation experiments with *Trp53*$^{+/-}$ mice, 6–10-week-old male and female mice from the 129-*Trp53tm1Tyj* strain were used. All animal experiments were performed in accordance with ethical and legal regulations for animal welfare and approved by the governmental council (Regierungspräsidium Karlsruhe, Germany).

In vivo Radiation and Chemotherapy

Prior to cerebellum particle irradiation, mice were anaesthetized by inhalation anesthesia, a mixture of 2% isoflurane with 2 L/min flow rate compressed medical air. The whole cerebellum, 7 × 7 mm region around the cell injection site was irradiated with 3 Gy of carbon ions or protons for 5 consecutive fractions at HIT. For details of radiation, PARPi and chemotherapy treatment see Supplementary Methods.

Histology, PARP Pharmacodynamic Activity, PARPi-FL Blocking Study, Bioinformatic Analysis, Magnetic Resonance Imaging

See Supplementary Methods.

Results

To evaluate the benefits of particle therapy and PARPi for medulloblastomas with chromothripsis, we tested this approach in vitro and in PDX models derived from matched primary and relapsed tumor cells.

We first tested particle therapy alone and in combination with the recently developed PARPi BGB290 in medulloblastoma cells with chromothripsis. We selected a p53-deficient chromothriptic medulloblastoma cell line (DAOY) and applied different doses of proton or CIRT with or without addition of BGB290. We used talazoparib as a positive control for in vitro experiments, due to the high potency of this PARPi. Both types of particle radiation led to a dose-dependent decrease in the metabolic activity of the cells, with CIRT being more potent than protons (Figure 1a and b). At 2, 4, and 6 Gy of proton irradiation, BGB290 addition led to a significant decrease in the metabolic activity of the cells as compared to proton irradiation alone. CIRT was very potent as a single treatment and the added benefit of BGB290 was only significant at 2 Gy (Figure 1b). For comparison, we also applied BGB290 in combination with the topoisomerase inhibitor topotecan, which is used in clinical studies in combination with PARPi.[35] At 10 nM topotecan, BGB290 addition led to a significant decrease in the metabolic activity of the cells as compared to topotecan alone (Figure 1c). To confirm the effects of DNA damage in combination with BGB290 in additional medulloblastoma models with chromothripsis, we generated spheroid cultures from six PDX models from four patients. Importantly, BGB290 with topotecan led to a significant reduction in the metabolic activity of the cells as compared to topotecan alone (Figure 1d). Altogether, particle radiation and topotecan alone as well as in combination with PARPi showed promising results in vitro.

Before moving on to in vivo models, we tested whether the primary tumors and PDX models investigated here were susceptible to PARPi at all. We showed that

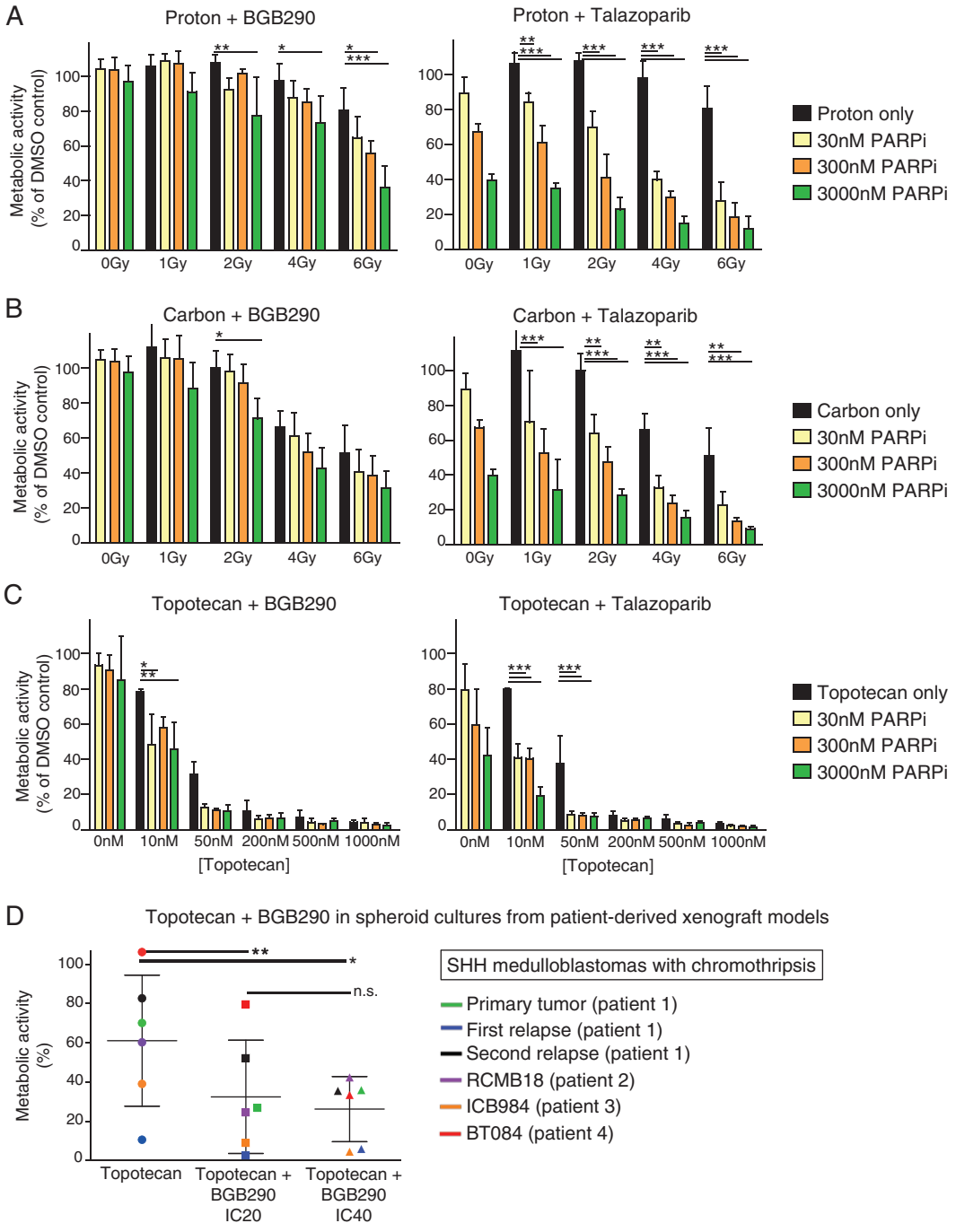

Fig. 1 Effects of particle radiation, topotecan and combination with PARPi in human medulloblastoma cells (DAOY) (a–c) and in spheroids from PDX models (d, each model shown in a different color, with the first three models derived from one patient). Metabolic activity was determined 72h (a–c) or 96 h (d) after treatment start. For statistical comparison between single and combination treatment effects, two-way ANOVA was performed in a–c and paired *t* tests were performed in d (*$P < .05$, **$P < .01$, ***$P < .001$).

medulloblastomas with chromothripsis have a significantly higher HR deficiency (HRD) score as compared to medulloblastomas without chromothripsis from the same molecular subgroup (Figure 2a). In addition, the exposure for COSMIC mutational signature ID8, characteristic of DNA DSB repair by nonhomologous end-joining and linked with HRD,[36] was significantly higher in medulloblastomas with chromothripsis as compared to other medulloblastomas from the same molecular subgroup (Figure 2b). RNA sequencing of tumor tissue showed that *PARP1* is expressed at high levels in medulloblastomas from this molecular subgroup (Sonic Hedgehog, SHH) (Figure 2c). Furthermore,

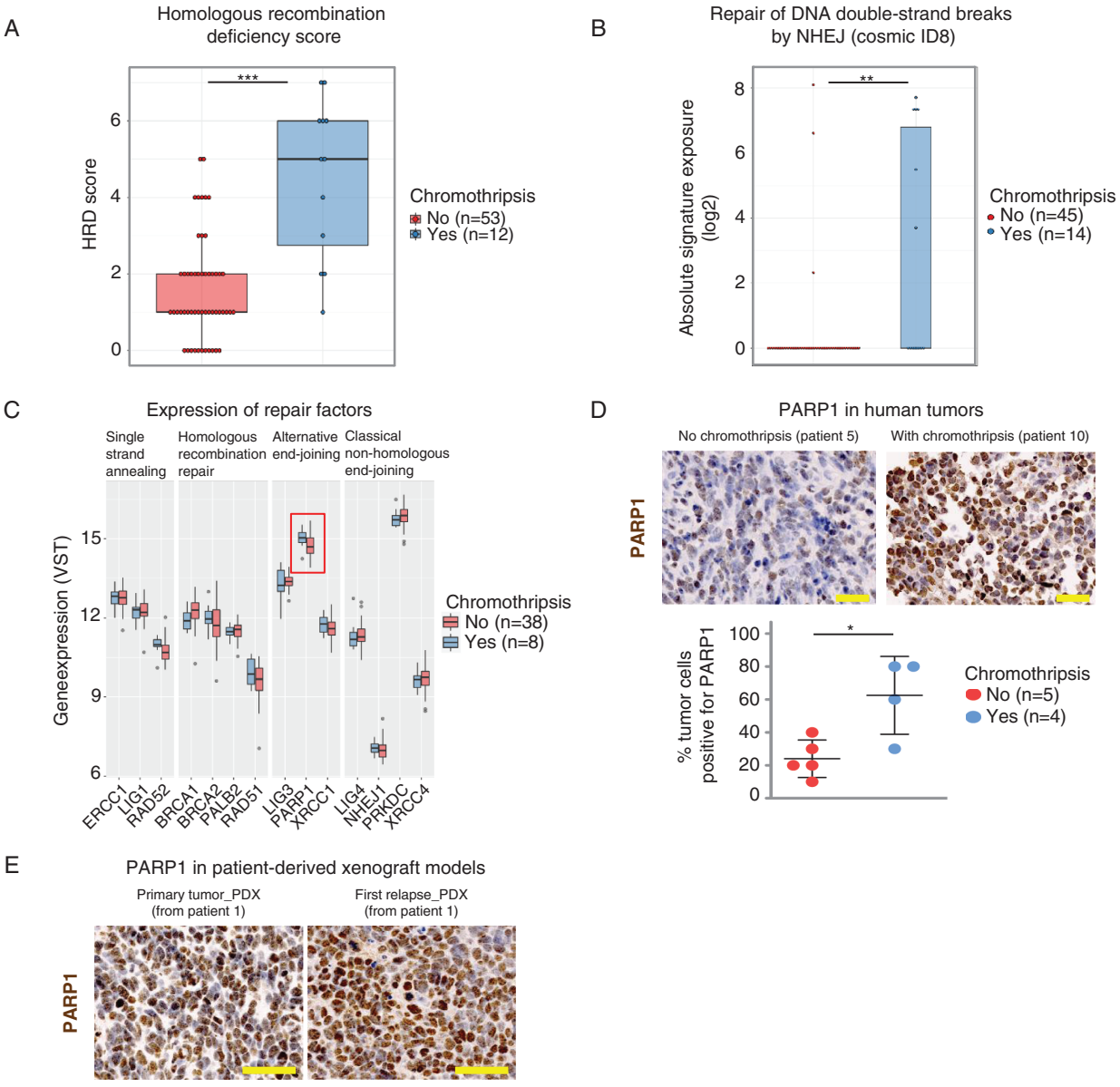

Fig. 2 Rationale for the use of PARPi in SHH medulloblastomas with chromothripsis. (a) HRD score in SHH medulloblastomas with and without chromothripsis (Wilcoxon-test, ***$P < .0001$). (b) Exposure to indel signature 8, linked to DNA DSB repair by NHEJ (Wilcoxon-test, **$P < .01$). (c) Expression levels of repair factors (RNA-sequencing) in SHH medulloblastomas showing elevated *PARP1* expression. *PARP1* expression is not significantly different between SHH medulloblastomas with and without chromothripsis at RNA level. (d) PARP1 expression (immunohistochemistry) in SHH medulloblastomas with and without chromothripsis (*$P = .0142$, unpaired *t* test) . (e) PARP1 expression (immunohistochemistry) in primary tumor and first relapse PDX models of a SHH medulloblastoma-LFS patient. Scale bars: 40 µm. NHEJ, Non-Homologous End-Joining.

immunohistochemical analyses showed homogenous high expression of PARP1 in SHH medulloblastomas with chromothripsis (Figure 2d, Supplementary Figure 1) and in orthotopic PDX models with chromothripsis (derived from a primary and relapse tumor from the same patient, Figure 2e), suggesting that these models can be used to test radiation in combination with PARPi.

For preclinical in vivo studies in medulloblastoma PDX models, blood-brain barrier penetrant PARPi are needed. Due to its poor blood-brain barrier penetrance, the widely used PARPi talazoparib is problematic in the context of brain tumors. We tested the inhibitory effect on the enzymatic activity of PARP1 and the blood-brain barrier penetrance of BGB290, a recently developed PARPi.[37] PARP enzyme activity quantification showed that at a 10 nM concentration, BGB290 offers the same range of inhibition of PARP enzyme activity as talazoparib, a potent but poorly brain-penetrant PARPi (Supplementary Figure 2a). To test

for blood-brain barrier penetrance of PARPi, in vivo competition assays with a fluorescently labeled PARPi (PARPi-FL) can be used.[38] To probe the BGB290 uptake in brain xenografts, we injected BGB290 into xenograft-bearing mice before PARPi-FL addition. This significantly reduced the uptake of the fluorescent imaging agent by 25% ($P < .05$), confirming that BGB290 crosses the blood-brain barrier (Supplementary Figure 2b).

We next applied particle radiation or chemotherapy (topotecan) with PARPi in preclinical mouse models of medulloblastoma. First, we tested the effects of the radiation alone in a highly aggressive model that we established from medulloblastoma cells from a heavily pretreated patient, who had received chemo- and radiotherapy. When the implanted tumors had reached a predefined size-threshold based on MRI measurements, we randomized the mice and applied five fractions of CIRT (5 × 3Gy) to the cerebellum in the treated group. Remarkably, this 5-day treatment was sufficient to delay tumor growth by 53 days (median survival: 96 days in treated animals; 43 days in controls), providing a highly significant survival benefit (Figure 3a). In contrast, topotecan alone or in combination with BGB290 did not lead to any survival benefit in the same model (Supplementary Figure 3). Encouraged by these promising results with CIRT in a pretreated tumor, we then used the patient-derived model of the matched untreated primary tumor and tested the effect of PARPi in addition to CIRT or proton radiation (Figure 3b). PARPi alone did not lead to any benefit as compared to the control group. In contrast, proton irradiation (5 × 3Gy) led to a significant improvement in survival (85 vs 52 days, $P < .01$). The addition of BGB290 to proton irradiation significantly improved the survival as compared to proton alone (96 vs 85 days, $P < .05$). The most striking results were obtained with CIRT, which led to a complete response in 79% of the animals (11 out of 14) based on MRI and histology (Figure 3c, Supplementary Figure 4). Three CIRT mice showed a tumor regrowth, two of them over 180 days after the 5-day treatment and one after 60 days. The remaining 11 animals were tumor-free, with four of them being sacrificed due to age-related issues or other tumor-independent issues such as vaginal prolapse. The 11 cured animals remained tumor-free for up to 300 days after the 5 days of irradiation. Additional benefits of PARPi were possibly hidden by the strong CIRT effect. Therefore, we investigated the mechanism of action of CIRT in the two PDX models.

For our initial in vivo experiment with carbon ions (pilot study, Figure 3a), we used three different strains of immunocompromised mice (NSG, NRGS and BALB/c-nude) for the following reasons. First, NSG mice, which are commonly used for PDX models, are radiation-sensitive and may not tolerate high doses of radiation well due to the DNA-PK knockout.[39] Second, potential treatment effects on the tumor growth in these animals may be linked with the death of surrounding damage-sensitive mouse cells rather than with direct effects of the treatment on xenotransplanted human tumor cells. NSG mouse cells, in contrast to the cells of NRGS or BALB/c mice, lack a functional nonhomologous end-joining repair process,[39] and comparing strains gives hints to which repair processes rejoin radiation-induced DNA breaks. Including both radiation-sensitive and radiation-tolerant mouse strains also allowed testing the effects of the treatment and side-effects on normal tissue in an LFSlike context. At the applied radiation dose, animals from all three strains showed similar survival benefits (Figure 3a). However, the molecular effect of the treatment on cells surrounding the tumor differed substantially between the mouse strains (Figure 4). We examined the brains of these mice and performed hematoxylin and eosin stains, STEM121 stains to identify human cells in the mouse brains as well as immunofluorescence analyses of γH2AX (marker of DNA DSBs) and RAD51 (HR repair factor). We quantified the signals within the radiation field (cerebellum, mostly containing human tumor cells), in the mouse cells directly surrounding the tumor (within the irradiated cerebellum), in the cortex close to the irradiation field and in the frontal cortex (far from the targeted irradiation field, Figure 4a).

Xenografted human tumor cells showed similar levels of DNA DSBs across mouse strains and also across treated and untreated animals, suggesting that the vast majority of DNA DSBs observed more than 70 days after the radiation were tumor-cell intrinsic (Figure 4b, left panel). In NRGS and BALB/c mice, we detected only very few γH2AX-positive mouse cells in the cerebellum and in the cortex, suggesting that DNA DSBs were already repaired at this stage or that damaged cells were successfully eliminated. In contrast, NSG mice showed significantly higher levels of DNA DSBs in CIRT animals as compared to control animals, with massive unrepaired damage in the cerebellum, but also some damage in the cortex, even more than 70 days after treatment. Unrepaired DNA DSBs in NSG animals suggest that carbon ion-induced damage was at least partly repaired by nonhomologous end-joining, as this repair process is inactive in NSG mice. As expected for tumors showing high HR deficiency scores, RAD51-positive cells were very rare, with <40% of the cells showing at least one signal per nucleus shortly after irradiation (Figure 4c). More than 70 days after the treatment, we detected even fewer cells with RAD51 foci, with levels of positive cells in the same range as for the control animals.

As CIRT achieved long-term local tumor control in this aggressive primary medulloblastoma model, we sought to investigate potential side-effects in the normal tissue in cured mice. For children with brain tumors receiving radiation, impaired cognitive function and neurological development represent a major issue. Therefore, we quantified neurogenesis in the dentate gyrus of the hippocampus of CIRT-treated and control mice. For this, we performed immunofluorescence analyses of doublecortin, an established marker of newborn neurons. Importantly, the numbers of newborn neurons in the dentate gyrus were not significantly different between control and treated animals (Figure 5a). The general neurological function of the mice cured by CIRT was not noticeably affected, as the animals moved and behaved normally. The brain morphology of the CIRT animals presented a normal appearance based on MRI and histology. Quantification of the brain volumes over time did not show any significant difference between control and treated animals due to radiation (Figure 5b). The only significant change in brain volume was an increase in control animals due to the tumor growth. In addition to possible consequences on the brain function, another potential side-effect of radiation is the induction of

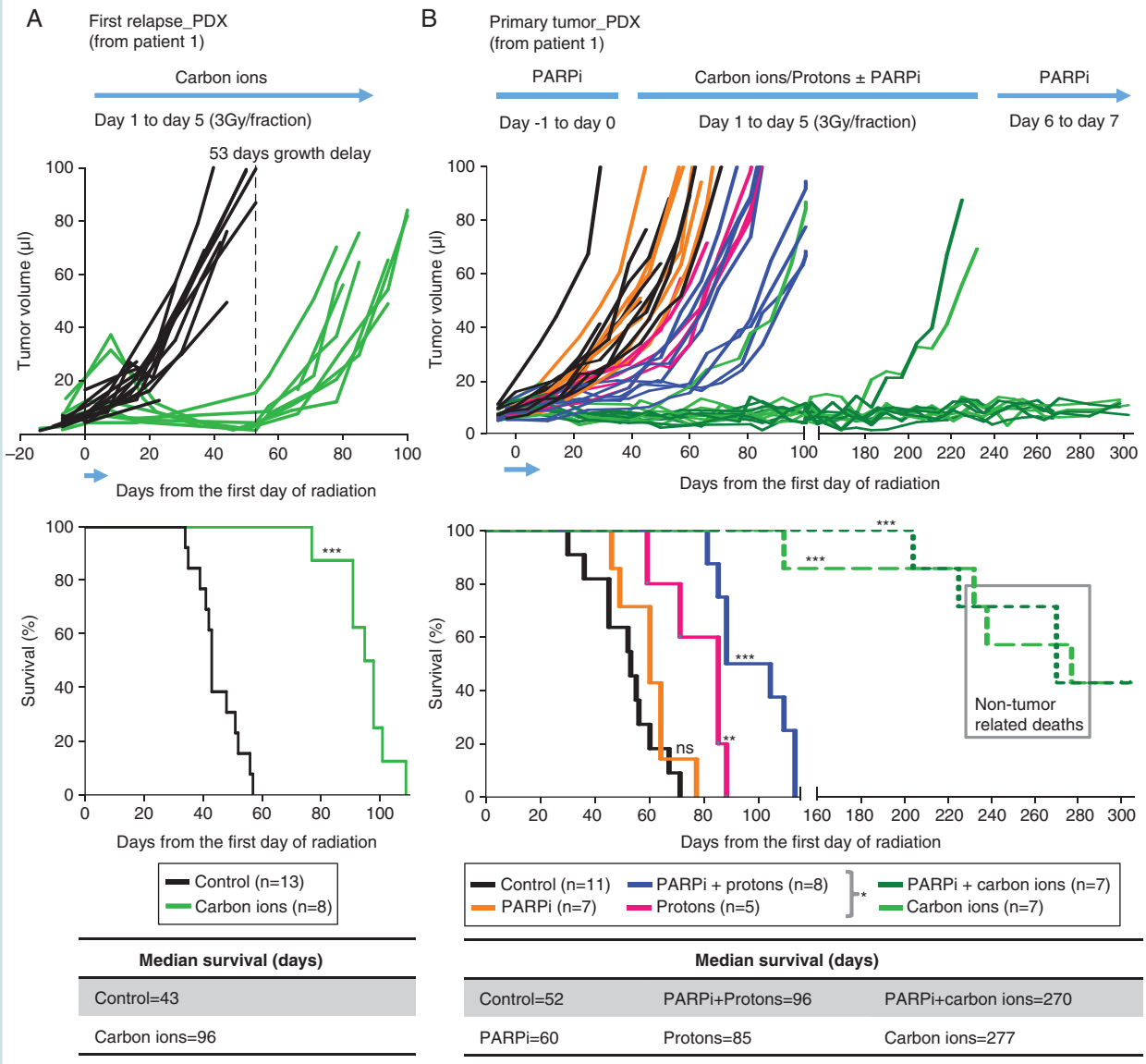

Median survival (days)
Control=43
Carbon ions=96

Median survival (days)		
Control=52	PARPi+Protons=96	PARPi+carbon ions=270
PARPi=60	Protons=85	Carbon ions=277

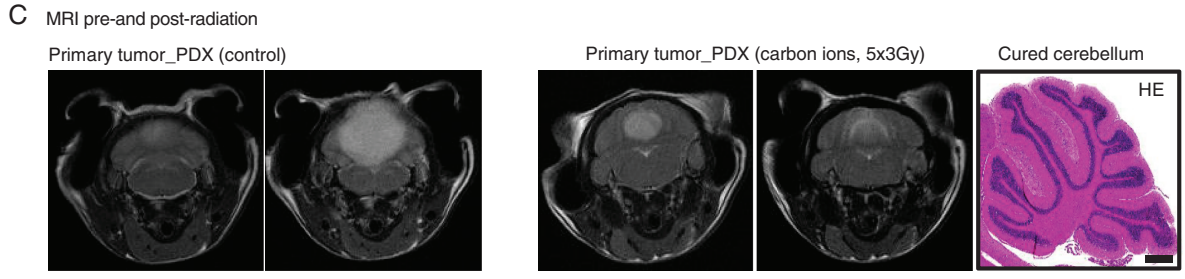

Fig. 3 Effects of fractionated particle radiation (5 × 3 Gy) alone or in combination with PARPi BGB290 on tumor growth and survival in matched first relapse (a, $n = 13$ for controls and $n = 8$ for carbon ions) and primary tumor (b, $n = 11$ for controls, 7 for PARPi, 8 for PARPi + protons, 5 for protons, 7 for PARPi + carbon ions, 7 for carbon ions) PDX models from a SHH medulloblastoma-LFS patient. The results of log-rank (Mantel-Cox) tests on Kaplan–Meier curves indicate the survival benefit of each treatment group in comparison to control (*$P < .05$, **$P < 01$, ***$P < .0001$). (c) Representative MRI images of PDX brains pre- and postradiation. A representative image of hematoxylin and eosin (HE) stain shows the cerebellum in CIRT animal after the complete response to irradiation. Scale bar: 500 µm.

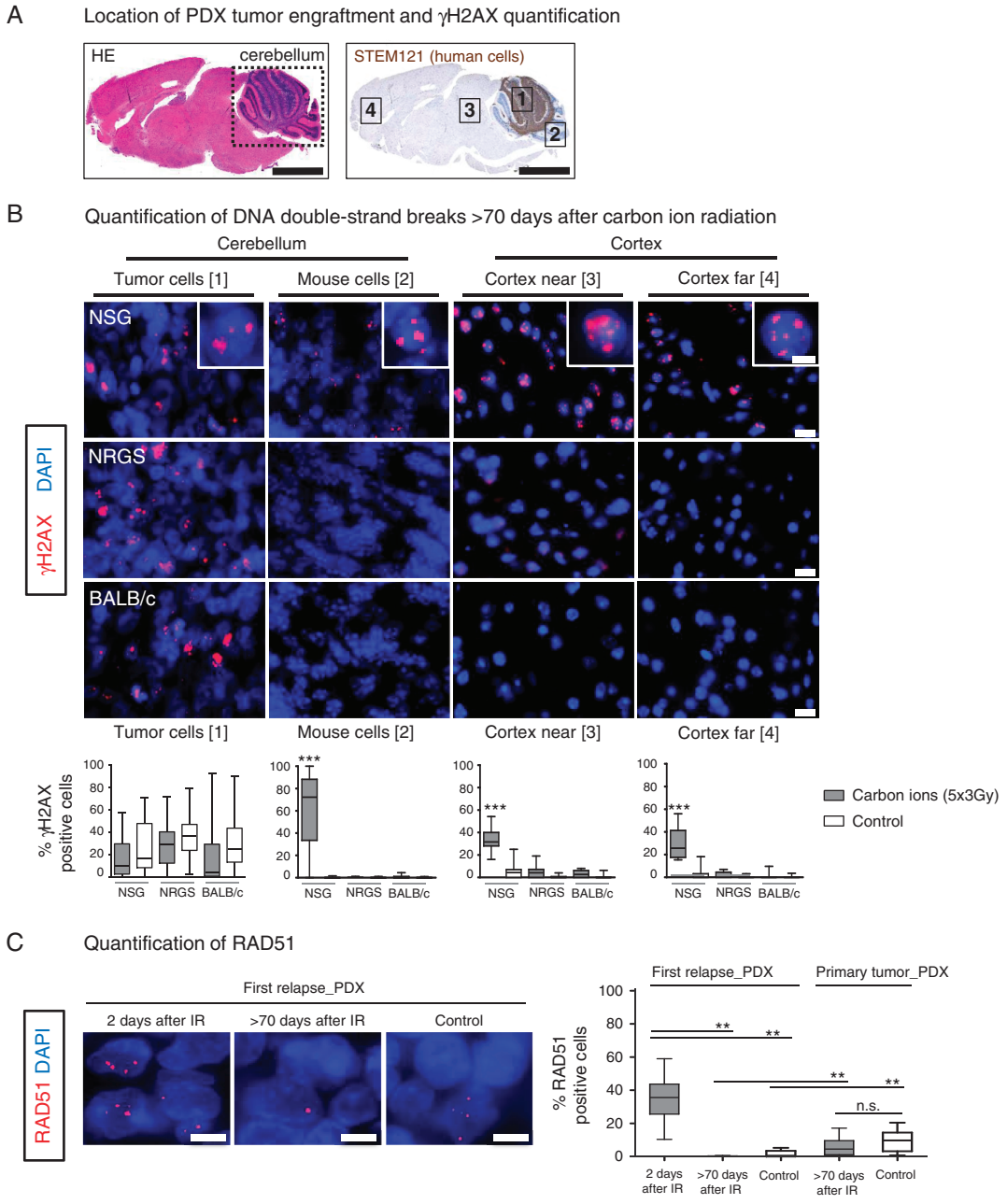

Fig. 4 Molecular analysis of brain tissues after fractionated CIRT (5 × 3 Gy) in the first relapse PDX mouse model of SHH medulloblastoma. (a) Hematoxylin and eosin and STEM121 (human cell marker) stains show the location of xenografted cells. Scale bars: 2.5 mm. (b) DNA damage >70 days after CIRT (5 × 3 Gy) remains unrepaired in the mouse cells of NSG animals. Quantification and comparison of DNA damage repair between irradiated and control mice at the survival endpoints (two-tailed Mann–Whitney test ***$P < .0001$) in brain locations shown in (a). Scale bars: 5 µm (magnified image) and 10 µm. (c) RAD51 scoring in tumor cells of control and CIRT PDX brains of NRGS mice. Scale bars: 5 µm.

secondary tumors. Therefore, we analyzed brain MRI data from all animals (Figure 5c, Supplementary Figure 5a). We did not detect any putative radiation-induced secondary tumor in the CIRT mice (up to 300 days after treatment). In the pilot cohort from the pretreated model for which the tumor regrew after 96 days, neuropathological evaluation did not show any significant difference between control and CIRT animals in terms of number of mice with necrosis within the tumors and there was no necrosis outside the tumors (Supplementary Figure 5b). Neuropathological analysis also confirmed the normal cerebellum structure and the absence of neuronal loss, disruption of the tissue architecture or fibrosis in cured animals (Supplementary Figure 5c). Immunohistochemical analyses were done for STEM121 to detect putative remaining human cells, GFAP as astrocyte marker and Ki67. This showed that the few

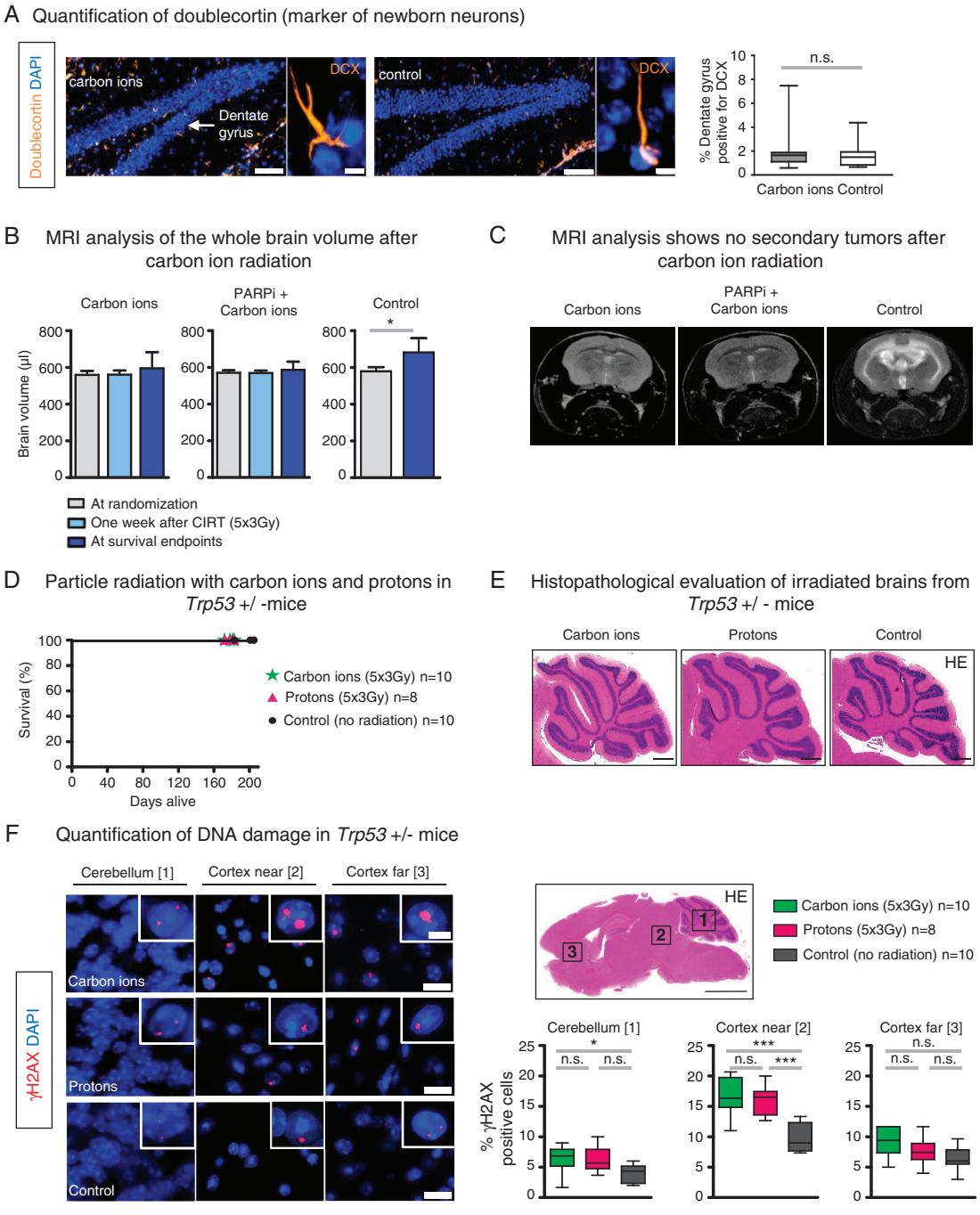

Fig. 5 Analysis of putative long-term side-effects of CIRT. (a) Quantification of doublecortin (marker of newborn neurons) and comparison between irradiated (n = 5 mice, 240–270 days postirradiation) and control animals (n = 5 mice, 50–60 days postrandomization) (two-tailed Mann–Whitney test, P = .7). Immunofluorescent staining and quantification of DCX in the dentate gyrus was done on three to five sagittal brain sections per animal. Scale bars: 5 µm (magnified neuron) and 100 µm. (b) Quantification of the brain volumes (n = 7 mice for carbon ions, n = 7 mice for PARPi + carbon ions and n = 11 mice for controls) (c) A representative T2-weighted image (corresponding to 1 from 20 slices taken per animal) from each treatment group. No radiation-induced tumor could be detected in any of the CIRT animals (with or without PARPi addition). (d) Overall survival of *Trp53*$^{+/-}$ mice after particle radiation. (e) Histopathological analysis shows a normal cerebellum structure for *Trp53*$^{+/-}$ mice (representative images for each group). Scale bars: 500 µm. (f) Quantification of cells positive for DSB marker γH2AX in *Trp53*$^{+/-}$ mice (one-way ANOVA, $^{*}P < .05$, $^{***}P < .0001$). Scale bars: 5 µm (magnified cell) and 10 µm, 2.5 mm (HE image).

remaining human cells in the cured animals form no tumor remnants but foci of cerebellar gliosis, with intense GFAP immunostaining containing reactive astrocytes and compact glial fibers, suggesting posttreatment pathomorphosis (Supplementary Figure 5c). Even in repair-deficient NSG mice that are closer to the p53-deficient context as compared to NSG or nude mice, no secondary tumor was detected within the observation period.

To evaluate putative side-effects to the normal brain in the context of p53 inactivation, we applied proton irradiation or CIRT to the cerebellum of *Trp53*$^{+/-}$ mice (5 × 3Gy, Figure 5d). Importantly, MRI and neuropathology analyses did not detect any tumor lesion, after 200 days of follow-up (Figure 5e). The brain structure of treated animals (n = 10 for carbon ions and n = 8 for protons) was indistinguishable from that of control animals (n = 10) (Figure 5e). We quantified DNA DSBs in the irradiated area, close to the irradiated area and in the frontal cortex (far from the irradiated area). This analysis showed only minor differences in the percentage of cells positive for γH2AX (5% for controls and 6%–7% for treated mice in the irradiated cerebellum, Figure 5f).

Altogether, CIRT provided an effective treatment strategy in the primary PDX model, with favorable toxicity profile even in NSG mice showing unrepaired DSBs. As in the pretreated model the tumors started regrowing after 53 days, we performed high-coverage whole-genome sequencing (60x) to get insights into the genomic profile and clonal composition of the regrowing tumors (Figure 6). We did not detect any major change in somatic CNVs after irradiation (Figure 6a). On chromosomes 8 and 12, we observed a less deep coverage drop after irradiation, suggesting a minor enrichment for a clone without any loss on these two chromosomes. No increase in SVs was detected postradiation, with only two breakpoints present in the irradiated sample but not in the control sample. Therefore, cells with high amounts of radiation-induced DNA breaks likely died or were present in a proportion below the detection limit. The high similarity between the genomic profiles of the control and CIRT cells was further supported by the comparable growth kinetics of the tumors, with no significant difference in the slopes (doubling times of 16 and 17.5 days, respectively), despite a growth delay of 53 days postirradiation (Figure 6b). Similar growth rates supported the absence of major treatment-induced clonal shift and suggested no significant increase in aggressiveness after CIRT. Next, we analyzed clonal and subclonal SNVs to further characterize the composition of the regrowing tumors. The clonal composition did not change significantly, after irradiation, with only minor shifts detected based on allele frequency analysis (Figure 6c). Private somatic mutations detected only in the control or only in the irradiated cells were rare (121 and 272, respectively, Figure 6d).

Neutral tumor evolution was linked with power-law distributions of mutant allele frequencies.[40] For untreated tumor cells, the linear distribution of mutations suggested potential neutral tumor evolution, indicating that all clonal selection might have occurred before the onset of cancer growth and not in later arising subclones (Figure 6d). In contrast, after irradiation, the measured distribution deviated from the distribution expected under neutral evolution, which could possibly reflect a change in mutation rate, cell survival or clonal selection. As daughter cells were likely killed during the treatment, only the outcome of final cell divisions was observed in the DNA sequence, leading to apparently higher mutation rates. Importantly, the fractions of tumor stem cells (SOX2-positive) and proliferating cells (Ki67-positive) were comparable between control and irradiated animals, after the tumors had regrown (Supplementary Figure 6), suggesting that radioresistant cancer stem cells might have reconstituted the tumors, with similar features to the original tumors. In line with this, the modeling indicated that 10% of the tumor cells may have survived the treatment.

To conclude, we identified an efficient local therapy intensification strategy with CIRT to treat primary medulloblastomas with chromothripsis in preclinical models. Further options to overcome radioresistance of pretreated and relapsed tumors will be needed, to achieve similar tumor control rates in the relapse setting as observed in treatment-naïve tumors.

Discussion

We assessed different approaches to meet the needs for highly precise treatments targeting the tumor cells, while utilizing the HR repair defects of medulloblastomas with chromothripsis.

Remarkably, CIRT led to a complete response for the vast majority (79%) of the animals harboring treatment-naïve orthotopic medulloblastoma of the highly aggressive *TP53*-mutant chromothriptic subgroup. The experimental set-up was close to the situation in the clinic, with a treatment start well, after tumor onset. Importantly, the applied fractionated CIRT regimen was comparable to therapeutic settings in humans, as similar or even higher doses are applied to patients.[41]

Therefore, further investigation of CIRT to eradicate aggressive medulloblastomas developing in LFS patients is warranted, and more broadly in the context of pediatric oncology. High precision, that is, sparing of normal tissue has been attributed to reduced risk of secondary cancer, after proton therapy and CIRT.[42] Even though secondary malignancies cannot be formally excluded, we performed a long-term follow-up (300 days) and did not detect any. The low radiation dose received outside the target area (cerebellum) visible in NSG mice did not cause any radiation-induced tumor, despite the repair deficiencies of these animals. However, the impact of CIRT and germline *TP53* status needs to be further explored as densely ionizing space irradiation was shown to enhance tumor formation in p53-null breast tissue background.[43] Further detailed analyses will be required before clinical applications (eg, additional experiments in p53-deficient genetic mouse models, deeper evaluation of the impact on neurologic performance, behavioral experiments to assess neurocognitive function) to exclude any side-effect that remained undetected at this stage. Furthermore, the benefits from the addition of a PARPi to reduce the radiation dose need to be further explored.

An important aspect is the specificity of the carbon ion effects to chromothriptic cells, to medulloblastoma

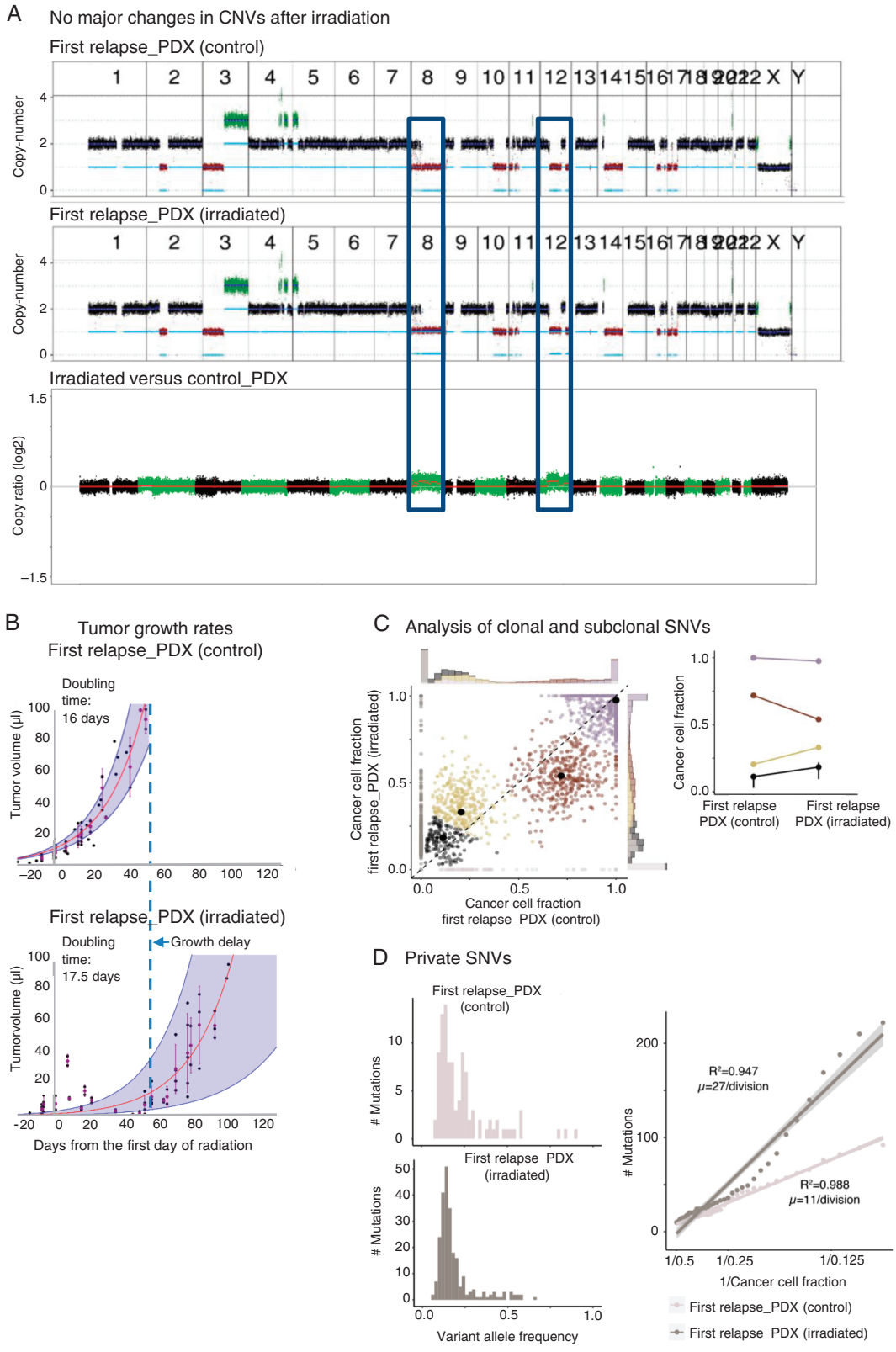

Fig. 6 Whole-genome sequencing analysis of re-grown tumors from the first relapse PDX model after CIRT. (a) CNV comparison between carbon ion treated (91 days postirradiation) and control animal from the first relapse model. (b) Tumor growth rates and doubling times in the control and CIRT tumors. (c) Analysis of clonal and subclonal SNVs shows no major clonal shift after CIRT. (d) Rare private mutations detected only in the control or in the irradiated sample. In a neutrally and exponentially expanding population, mutations accumulate according to a power-law-distribution, which would be supported in the control sample. After irradiation, the small R^2 suggests a deviation from the power-law.

cells with chromothripsis and to tumor cells with HR deficiency. A similar strategy did not cure the mice in a glioblastoma xenograft model[44] or in a genetically engineered mouse model of soft tissue sarcoma,[45] suggesting that this approach does not have a general pan-tumor effect. In prostate cancer and in medulloblastoma, Konings and colleagues showed in vitro that carbon ions were more effective in decreasing cell survival and migration as compared to X-rays or proton.[46] It will be essential to further investigate the specificity of the biological effects of CIRT in chromothriptic medulloblastoma.

Even though the treatment was successful in the context of untreated primary medulloblastoma, the same strategy applied to the matched PDX model established from the posttreatment relapsed tumor led to a significant benefit but eventually relapse. There are several reasons for radioresistance, with one important source being cancer stem cells.[47] Immunofluorescence analysis showed the presence of cancer stem cells in both the primary tumor and in the relapse. Treatment-naïve cancer stem cells did not seem to be a major issue here, as shown by the high complete response rate to CIRT. However, tumors raised after previous radiotherapy exposure, as in the matched PDX from the relapsed tumor investigated here, acquired relative resistance to CIRT leading to tumor relapses, after a growth delay phase. Importantly, we detected no major clonal shift and no significant induction of genome rearrangements after CIRT, suggesting that the regrowing tumors were very similar to the initial tumors. Higher radiation doses to overcome putative radioresistant stem cells would go along with more side-effects, suggesting the need for a combination treatment targeting cancer stem cells.

Altogether, this study bears the potential to identify new therapeutic approaches for this challenging subgroup of patients. Tumor vulnerabilities to CIRT, like HRD and chromothripsis or more broadly genome instability in medulloblastoma demonstrated here may pave the way for the development of novel strategies.

Supplementary Material

Supplementary data are available at *Neuro-Oncology* online.

Keywords

carbon ion radiotherapy | chromothripsis | medulloblastoma | PARP inhibitor | synthetic lethality

Acknowledgments

We thank Peter Lichter, Peter Angel, and Magnus von Knebel Doeberitz for discussions. Anne Catrin Kittler, Frauke Devens, Michaela Hergt are acknowledged for generous support with immunofluorescence analyses. The DKFZ Light Microscopy facility, and especially Damir Krunic, is acknowledged for help with macro design. Sabrina Kirschner, Hermann Stammer, Viktoria Eichwald, Inna Babushkina, and Manuel Fischer are acknowledged for help with MRI. Sebastian Brabetz is acknowledged for advice on PDX. The DKFZ Core facility is acknowledged for support with sequencing. Caroline Pabst is acknowledged for sharing NRGS mice and Kerstin Dell for advice on animal experiments. Yanxin Wei is acknowledged for sharing protocol for spheroid culture. We thank Christian Brand from Summit Biomedical Imaging and Thomas Reiner from Memorial Sloan Kettering Cancer Center for providing PARPi-FL and for helpful discussions (both are shareholders of Summit Biomedical Imaging).

Funding

We received funding from the Wilhelm Sander Foundation and from the Fritz Thyssen Foundation.

Conflict of interest statement. J. Debus: Research Grant; Siemens Health Care GmbH, Solution Akademia Gmbh, Viewray Inc., CRI The Clinical Research Institute GmbH, Accuray International Sari, RaySearch Laboratories AB, Vision RT Limited, Merck Serono GmbH, Astellas Pharma GmbH, Astra Zeneca GmbH, Egomed PLC Surrey Research Park, Quintiles GmbH, Pharmaceutical Research Associates Gm. A. Abdollahi: Research Grant; Merck KGaA, FibroGen, Bayer. Consulting/advisory Role; Roche, Merck KGaA, Merck Serono, FibroGen, BMS Brazil, Bayer Health, BioMedX.

Authorship statement. M.S., M.M., M.B., H.S.S., and U.K. planned and performed the experiments. J.K.L.W. and D.H. performed the bioinformatic analyses. V.K. and S.B. performed the mathematical modeling. A.K. performed the neuropathology evaluation. N.M. provided the support of in vivo experiments. S.B. provided the support of radiation experiments. M.J., M.O.B., S.H., and M.Be. performed the MRI analysis. T.H. supervised the mathematical modelling. M.Z. supervised the bioinformatic analyses. P.C.W. shared the mouse line. J.D., M.K., S.M.P., and A.A. handled the supervision and critical feed-back. A.E. handled the project design, supervision and manuscript writing. All authors discussed the results and contributed to the final manuscript.

References

1. Rausch T, Jones DT, Zapatka M, et al. Genome sequencing of pediatric medulloblastoma links catastrophic DNA rearrangements with TP53 mutations. *Cell*. 2012;148(1-2):59–71.
2. Stephens PJ, Greenman CD, Fu B, et al. Massive genomic rearrangement acquired in a single catastrophic event during cancer development. *Cell*. 2011;144(1):27–40.
3. Li Y, Schwab C, Ryan S, et al. Constitutional and somatic rearrangement of chromosome 21 in acute lymphoblastic leukaemia. *Nature*. 2014;508(7494):98–102.

4. Lee JJ, Park S, Park H, et al. Tracing oncogene rearrangements in the mutational history of lung adenocarcinoma. *Cell.* 2019;177(7):1842–1857.e21.
5. Luijten MNH, Lee JXT, Crasta KC. Mutational game changer: chromothripsis and its emerging relevance to cancer. *Mutat Res.* 2018;777:29–51.
6. ICGC/TCGA Pan-Cancer Analysis of Whole Genomes Consortium. Pan-cancer analysis of whole genomes. *Nature.* 2020;578:82–93.
7. Rode A, Maass KK, Willmund KV, Lichter P, Ernst A. Chromothripsis in cancer cells: an update. *Int J Cancer.* 2016;138(10):2322–2333.
8. Cortes-Ciriano I, Lee JJ-K, Xi R, et al. Comprehensive analysis of chromothripsis in 2,658 human cancers using whole-genome sequencing. *Nat Genet.* 2020;52(3):331–341.
9. Kloosterman WP, Koster J, Molenaar JJ. Prevalence and clinical implications of chromothripsis in cancer genomes. *Curr Opin Oncol.* 2014;26(1):64–72.
10. Waszak SM, Northcott PA, Buchhalter I, et al. Spectrum and prevalence of genetic predisposition in medulloblastoma: a retrospective genetic study and prospective validation in a clinical trial cohort. *Lancet Oncol.* 2018;19(6):785–798.
11. Kratz CP, Achatz MI, Brugières L, et al. Cancer screening recommendations for individuals with Li-Fraumeni syndrome. *Clin Cancer Res.* 2017;23(11):e38–e45.
12. Hendrickson PG, Luo Y, Kohlmann W, et al. Radiation therapy and secondary malignancy in Li-Fraumeni syndrome: a hereditary cancer registry study. *Cancer Med.* 2020;9(21):7954–7963.
13. Swaminathan M, Bannon SA, Routbort M, et al. Hematologic malignancies and Li-Fraumeni syndrome. *Cold Spring Harb Mol Case Stud.* 2019;5(1):a003210.
14. Schulz-Ertner D, Jäkel O, Schlegel W. Radiation therapy with charged particles. *Semin Radiat Oncol.* 2006;16(4):249–259.
15. Pompos A, Durante M, Choy H. Heavy ions in cancer therapy. *JAMA Oncol.* 2016;2(12):1539–1540.
16. Mohamad O, Sishc BJ, Saha J, et al. Carbon ion radiotherapy: a review of clinical experiences and preclinical research, with an emphasis on DNA Damage/Repair. *Cancers (Basel).* 2017;9(6):66.
17. Combs SE, Kessel K, Habermehl D, Haberer T, Jäkel O, Debus J. Proton and carbon ion radiotherapy for primary brain tumors and tumors of the skull base. *Acta Oncol.* 2013;52(7):1504–1509.
18. Blattmann C, Oertel S, Schulz-Ertner D, et al. Non-randomized therapy trial to determine the safety and efficacy of heavy ion radiotherapy in patients with non-resectable osteosarcoma. *BMC Cancer.* 2010;10:96.
19. Mohamad O, Imai R, Kamada T, Nitta Y, Araki N; Working Group for Bone and Soft Tissue Sarcoma. Carbon ion radiotherapy for inoperable pediatric osteosarcoma. *Oncotarget.* 2018;9(33):22976–22985.
20. Combs SE, Kessel KA, Herfarth K, et al. Treatment of pediatric patients and young adults with particle therapy at the Heidelberg Ion Therapy Center (HIT): establishment of workflow and initial clinical data. *Radiat Oncol.* 2012;7:170.
21. Chan DA, Giaccia AJ. Harnessing synthetic lethal interactions in anticancer drug discovery. *Nat Rev Drug Discov.* 2011;10(5):351–364.
22. Ratnaparkhe M, Wong JKL, Wei PC, et al. Defective DNA damage repair leads to frequent catastrophic genomic events in murine and human tumors. *Nat Commun.* 2018;9(1):4760.
23. Gröbner SN, Worst BC, Weischenfeldt J, et al.; ICGC PedBrain-Seq Project; ICGC MMML-Seq Project. Author correction: the landscape of genomic alterations across childhood cancers. *Nature.* 2018;559(7714):E10.
24. Powell SN, Kachnic LA. Roles of BRCA1 and BRCA2 in homologous recombination, DNA replication fidelity and the cellular response to ionizing radiation. *Oncogene.* 2003;22(37):5784–5791.
25. Evers B, Helleday T, Jonkers J. Targeting homologous recombination repair defects in cancer. *Trends Pharmacol Sci.* 2010;31(8):372–380.
26. Bryant HE, Schultz N, Thomas HD, et al. Specific killing of BRCA2-deficient tumours with inhibitors of poly(ADP-ribose) polymerase. *Nature.* 2005;434(7035):913–917.
27. Kaufman B, Shapira-Frommer R, Schmutzler RK, et al. Olaparib monotherapy in patients with advanced cancer and a germline BRCA1/2 mutation. *J Clin Oncol.* 2015;33(3):244–250.
28. Bundred N, Gardovskis J, Jaskiewicz J, et al. Evaluation of the pharmacodynamics and pharmacokinetics of the PARP inhibitor olaparib: a phase I multicentre trial in patients scheduled for elective breast cancer surgery. *Invest New Drugs.* 2013;31(4):949–958.
29. Pilié PG, Gay CM, Byers LA, O'Connor MJ, Yap TA. PARP inhibitors: extending benefit beyond BRCA-mutant cancers. *Clin Cancer Res.* 2019;25(13):3759–3771.
30. Albert JM, Cao C, Kim KW, et al. Inhibition of poly(ADP-ribose) polymerase enhances cell death and improves tumor growth delay in irradiated lung cancer models. *Clin Cancer Res.* 2007;13(10):3033–3042.
31. Russo AL, Kwon HC, Burgan WE, et al. In vitro and in vivo radiosensitization of glioblastoma cells by the poly (ADP-ribose) polymerase inhibitor E7016. *Clin Cancer Res.* 2009;15(2):607–612.
32. Donawho CK, Luo Y, Luo Y, et al. ABT-888, an orally active poly(ADP-ribose) polymerase inhibitor that potentiates DNA-damaging agents in preclinical tumor models. *Clin Cancer Res.* 2007;13(9):2728–2737.
33. Veneris JT, Matulonis UA, Liu JF, Konstantinopoulos PA. Choosing wisely: selecting PARP inhibitor combinations to promote anti-tumor immune responses beyond BRCA mutations. *Gynecol Oncol.* 2020;156(2):488–497.
34. Brabetz S, Leary SES, Gröbner SN, et al. A biobank of patient-derived pediatric brain tumor models. *Nat Med.* 2018;24(11):1752–1761.
35. Wahner Hendrickson AE, Menefee ME, Hartmann LC, et al. A phase I clinical trial of the poly(ADP-ribose) polymerase inhibitor veliparib and weekly topotecan in patients with solid tumors. *Clin Cancer Res.* 2018;24(4):744–752.
36. Alexandrov LB, Kim J, Haradhvala NJ, et al.; PCAWG Mutational Signatures Working Group; PCAWG Consortium. The repertoire of mutational signatures in human cancer. *Nature.* 2020;578(7793):94–101.
37. Xiong Y, Guo Y, Liu Y, et al. Pamiparib is a potent and selective PARP inhibitor with unique potential for the treatment of brain tumor. *Neoplasia.* 2020;22(9):431–440.
38. Irwin CP, Portorreal Y, Brand C, et al. PARPi-FL–a fluorescent PARP1 inhibitor for glioblastoma imaging. *Neoplasia.* 2014;16(5):432–440.
39. Saki M, Bhat K, Sodhi SS, Nguyen NT, Kornblum HI, Pajonk F. Effects of brain irradiation in immune-competent and immune-compromised mouse models. *Radiat Res.* 2020;193(2):186–194.
40. Williams MJ, Werner B, Barnes CP, Graham TA, Sottoriva A. Identification of neutral tumor evolution across cancer types. *Nat Genet.* 2016;48(3):238–244.
41. Combs SE, Nikoghosyan A, Jaekel O, et al. Carbon ion radiotherapy for pediatric patients and young adults treated for tumors of the skull base. *Cancer.* 2009;115(6):1348–1355.
42. Mohamad O, Tabuchi T, Nitta Y, et al. Risk of subsequent primary cancers after carbon ion radiotherapy, photon radiotherapy, or surgery for localised prostate cancer: a propensity score-weighted, retrospective, cohort study. *Lancet Oncol.* 2019;20(5):674–685.
43. Illa-Bochaca I, Ouyang H, Tang J, et al. Densely ionizing radiation acts via the microenvironment to promote aggressive Trp53-null mammary carcinomas. *Cancer Res.* 2014;74(23):7137–7148.

44 Chiblak S, Tang Z, Lemke D, et al. Carbon irradiation overcomes glioma radioresistance by eradicating stem cells and forming an antiangiogenic and immunopermissive niche. *JCI Insight*. 2019;4(2):e123837.

45. Brownstein JM, Wisdom AJ, Castle KD, et al. Characterizing the potency and impact of carbon ion therapy in a primary mouse model of soft tissue sarcoma. *Mol Cancer Ther*. 2018;17(4):858–868.

46. Konings K, Vandevoorde C, Belmans N, et al. The combination of particle irradiation with the hedgehog inhibitor GANT61 differently modulates the radiosensitivity and migration of cancer cells compared to X-ray irradiation. *Front Oncol*. 2019;9:391.

47. Baumann M, Krause M, Overgaard J, et al. Radiation oncology in the era of precision medicine. *Nat Rev Cancer*. 2016;16(4):234–249.